

Cross-Shape Attention for Part Segmentation of 3D Point Clouds

Marios Loizou^{1*} Dmitry Petrov^{2*} Melinos Averkiou¹ Evangelos Kalogerakis²
¹University of Cyprus / CYENS CoE Cyprus ²UMass Amherst

Abstract

We present a method that propagates point-wise feature representations across shapes within a collection for the purpose of 3D shape segmentation. This is achieved through a cross-shape attention operation that assesses the degree of interaction between points on different shapes and mediates feature propagation. For each test shape, our method finds shapes in an input collection that are suited for executing such cross-shape attention operations. The resulting point-wise feature representations lead to more consistent 3D shape segmentation results, as demonstrated in our experiments.

1. Introduction

Learning effective point-based representations is fundamental to shape understanding and processing. In recent years, there has been significant research in developing deep neural architectures to learn point-wise representations of shapes through convolution and attention layers, useful for performing high-level tasks, such as shape segmentation. The common denominator of these networks is that they output a representation for each shape point by weighting and aggregating representations and relations with other points within the same shape.

In this work, we propose a *cross-shape attention* mechanism that enables interaction and propagation of point-wise feature representations across shapes of an input collection. In our architecture, the representation of a point in a shape is learned by combining representations originating from points in the same shape as well as other shapes. The rationale for such approach is that if a point on one shape is related to a point on another shape e.g., they lie on geometrically or semantically similar patches or parts, then cross-shape attention can promote consistency in their resulting representations and part label assignments. We leverage neural attention to determine and weigh pairs of points on different shapes. We integrate these weights in our cross-

shape attention scheme to learn more consistent point representations.

Developing such cross-shape attention mechanism poses a number of technical challenges. First, performing cross-attention across all-pairs of shapes becomes prohibitively expensive for large input collections of shapes. Our method learns a measure that allows us to select a small set of other shapes useful for such cross-attention operations with a given input shape. For example, given an input office chair, it is more useful to allow interactions of its points with points of another structurally similar office chair rather than a stool. During training, we maintain a sparse graph (Figure 1), whose nodes represent training shapes and edges specify which pairs of shapes should interact for training our cross-shape attention mechanism. At test time, the shape collection graph is augmented with additional nodes representing test shapes. New edges are added connecting them to training shapes for propagating representations from relevant training shapes.

Our method also introduces a new variant of a sparse tensor network combining MinkowskiNet [9] and architectural insights from HRNet [57] for multi-resolution feature processing. We extend this backbone with our cross-shape attention layer and train our new architecture end-to-end for semantic shape segmentation.

In summary, our main technical contribution is a multi-resolution sparse tensor network along with an attention-based mechanism that enables point-wise feature interaction and propagation across shapes for more consistent segmentation. Our experiments indicate higher performance on the recent PartNet dataset [39]. Compared to the MinkowskiNet baseline, we found an improvement of 3.1% in part IoU on average for fine-grained shape segmentation evaluated in PartNet.

2. Related work

We briefly overview related work on 3D deep learning for point clouds. We also discuss cross-attention networks developed in other domains.

3D deep learning for processing point clouds. Several different types of neural networks have been proposed

* indicates equal contributions.

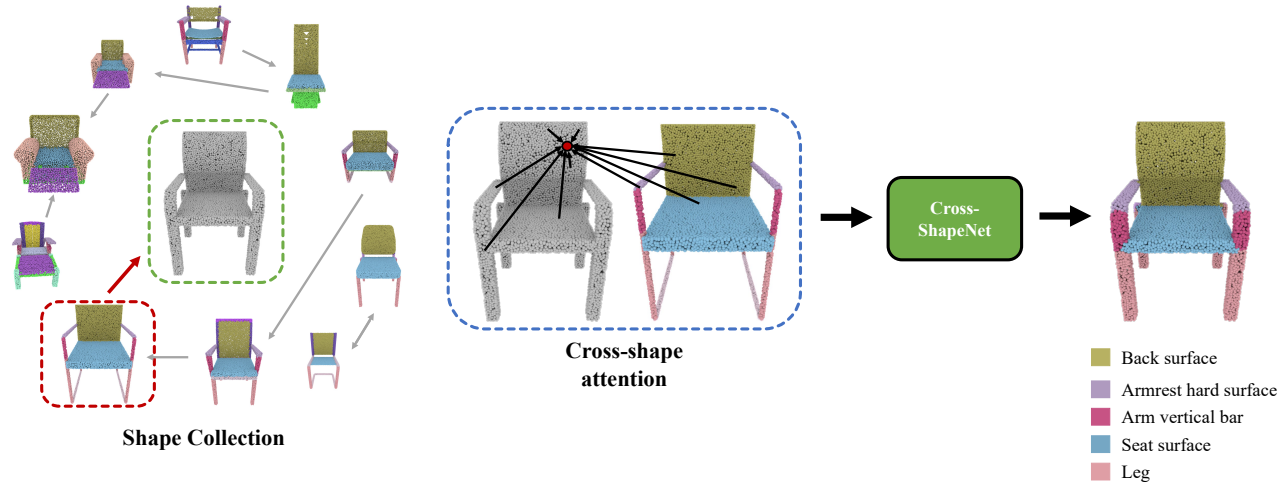


Figure 1. *Left*: given an input shape collection, our method constructs a graph, where each shape is represented as a node and edges indicate that shape pairs are deemed compatible for cross-shape feature propagation. *Middle*: At test time, our network (“CrossShapeNet”) computes point-wise feature representations for a test shape (grey shape) by allowing interaction with point-wise features from one or more training shapes through our proposed cross-shape attention mechanism. *Right*: As a result, the point-wise features of the test shape becomes more synchronized with the ones of relevant training shapes leading to more accurate fine-grained segmentation.

for processing point sets over the recent years. After the pioneering work of PointNet [42, 44], several works further investigated hierarchical point aggregation mechanisms to better model the spatial distribution of points [32, 51, 29]. Alternatively, point clouds can be projected onto local views [53, 43, 24, 20] and processed as regular grids through image-based convolutional networks. Another line of work converts point representations into volumetric grids [66, 37, 11, 45, 50, 36] and processes them through 3D convolutions. Instead of uniform grids, hierarchical space partitioning structures (e.g., kd-trees, lattices) can be used to define regular convolutions [46, 25, 59, 60, 52]. Another type of networks incorporate point-wise convolution operators to directly process point clouds [33, 19, 69, 34, 14, 1, 17, 61, 71, 65, 26, 54]. Alternatively, shapes can be treated as graphs by connecting each point to other points within neighborhoods in a feature space. Then graph convolution and pooling operations can be performed either in the spatial domain [64, 49, 27, 56, 74, 35, 28, 31, 23, 70, 58, 16, 29], or spectral domain [72, 3, 4, 41]. Attention mechanisms have also been investigated to modulate the importance of graph edges and point-wise convolutions [69, 70, 58, 73]. Graph neural network approaches have been shown to model non-local interactions between points within the same shape [64, 31, 70, 16]. Finally, several recent works [75, 15, 13, 38, 67] introduced variety of transformer-inspired models for point cloud processing tasks. None of the above approaches have investigated the possibility of extending attention across shapes. A notable exception are the methods by Wang et al. [63] and Cao et al. [5] that propose cross-attention mechanisms across

given pairs of point cloud instances representing different transformations of an underlying shape for the specific task of rigid registration.

Our method instead introduces cross-attention across shapes within a large collection without assuming any pre-specified shape pairs. Our method aims to discover useful pairs for cross-shape attention and learns representations by propagating them within the shape collection. Our method shows that the resulting features yield more consistent 3D shape segmentation than several other existing point-based networks.

Cross-attention in other domains. Our method is inspired by recent cross-attention models proposed for video classification, image classification, keypoint recognition, and image-text matching. Wang et al. [62] introduced non-local networks that allow any image query position to perceive features of all the other positions within the same image or across frames in a video. To avoid huge attention maps, Huang et al. proposes a “criss-cross” attention module [21] to maintain sparse connections for each position in image feature maps. Cao et al. [6] simplifies non-local blocks with query-independent attention maps [6]. Lee et al. [30] propose cross-attention between text and images to discover latent alignments between images regions and words in a sentence. Hou et al. [18] models the semantic relevance between class and query feature maps in images through cross-attention to localize more relevant image regions for classification and generate more discriminative features. Sarlin et al. [48] learns keypoint matching between two indoor images from different viewpoints

by leveraging self-attention and cross-attention to boost the receptive field of local descriptors and allow cross-image communication. Chen et al. [7] propose cross-attention between multiscale representations for image classification. Finally, Doersch et al. [12] introduced a CrossTransformer model for few-shot learning task on images. Give an unlabeled query image, their model computes local cross-attention similarities with a number of labeled images and then infers class membership.

Our method instead introduces attention mechanisms across 3D shapes. In contrast to cross-attention approaches in the above domains, we do not assume any pre-existing paired data. The usefulness of shape pairs is determined based on a learned shape compatibility measure.

3. Method

Given an input collection of 3D shapes represented as point clouds, the goal of our method is to extract and propagate point-based feature representations from one shape to another, and use the resulting representations for 3D semantic segmentation. To perform the feature propagation, we propose a Cross-Shape Attention (CSA) mechanism. The mechanism first assesses the degree of interaction between pairs of points on different shapes. Then it allows point-wise features on one shape to influence the point-wise features of the other shape based on their assessed degree of interaction. In addition, we provide a mechanism that automatically selects shapes (“key shapes”) to pair with an input test shape (“query shape”) to execute these cross-shape attention operations. In the following sections, we first discuss the CSA layer at test time (Section 3.1). Then we discuss our retrieval mechanism to find key shapes given a test shape (Section 3.2), our training (Section 3.3), test stage (Section 3.4), and finally our network architecture details (Section 3.5).

3.1. Cross-shape attention for a shape pair

The input to our CSA layer is a pair of shapes represented as point clouds: $\mathcal{S}_m = \{\mathbf{p}_i\}_{i=1}^{P_m}$ and $\mathcal{S}_n = \{\mathbf{p}_j\}_{j=1}^{P_n}$ where $\mathbf{p}_i, \mathbf{p}_j \in \mathcal{R}^3$ represent 3D point positions and P_m, P_n are the number of points for each shape respectively. Our first step is to extract point-wise features for each shape.

In our implementation, we used a sparse tensor network based on a modified version of MinkowskiNet [9], as a backbone for feature extraction (architecture details are provided in Section 3.5 and supplementary material). The output from the backbone is a per-point D -dimensional representation ($D = 256$ in our implementation) stacked into a matrix for each of two shapes respectively: $\mathbf{X}_m \in \mathcal{R}^{P_m \times D}$ and $\mathbf{X}_n \in \mathcal{R}^{P_n \times D}$. The CSA layer produces new D -

dimensional point-wise representations for both shapes:

$$\mathbf{X}'_m = f(\mathbf{X}_m, \mathbf{X}_n; \theta), \quad \mathbf{X}'_n = f(\mathbf{X}_n, \mathbf{X}_m; \theta) \quad (1)$$

where f is the cross-shape attention function with learned parameters θ described in the next paragraphs.

Key and query intermediate representations. Inspired by Transformers [55], we first transform the input point representations of the first shape in the pair to intermediate representations, called “query” representations. The input point representations of the second shape are transformed to intermediate “key” representations. The keys will be compared to queries to determine the degree of influence of one point on another. Specifically, these transformations are expressed as follows:

$$\mathbf{q}_{m,i}^{(h)} = \mathbf{W}_q^{(h)} \mathbf{x}_{m,i}, \quad \mathbf{k}_{n,i}^{(h)} = \mathbf{W}_k^{(h)} \mathbf{x}_{n,j} \quad (2)$$

where $\mathbf{x}_{m,i}$ and $\mathbf{x}_{n,j}$ are point representations for the query shape \mathcal{S}_m and key shape \mathcal{S}_n , $\mathbf{W}_q^{(h)}$ and $\mathbf{W}_k^{(h)}$ are $D' \times D$ learned transformation matrices shared across all points of the query and key shape respectively, and h is an index denoting each different transformation (“head”). The dimensionality of the key and query representations D' is set to $\lfloor D/H \rfloor$, where H is the number of heads. These intermediate representations are stacked into the matrices $\mathbf{Q}_m^{(h)} \in \mathcal{R}^{P_m \times D'}$ and $\mathbf{K}_n^{(h)} \in \mathcal{R}^{P_n \times D'}$. Furthermore, the point representations of the key shape \mathcal{S}_n are transformed to value representations as:

$$\mathbf{v}_{n,j}^{(h)} = \mathbf{W}_v^{(h)} \mathbf{x}_{n,j} \quad (3)$$

where $\mathbf{W}_v^{(h)}$ is a learned $D' \times D$ transformation shared across the points of the key shape. These are also stacked to a matrix $\mathbf{V}_n^{(h)} \in \mathcal{R}^{P_n \times D'}$.

Pairwise point attention. The similarity of key and query representations is determined through scaled dot product [55]. This provides a measure of how much one shape point influences the point on the other shape. The similarity of key and query representations is determined for each head as:

$$\mathbf{A}_{m,n}^{(h)} = \text{softmax} \left(\frac{\mathbf{Q}_m^{(h)} \cdot (\mathbf{K}_n^{(h)})^\top}{\sqrt{D'}} \right) \quad (4)$$

where $\mathbf{A}_{m,n}^{(h)} \in \mathcal{R}^{P_m \times P_n}$ is a cross-attention matrix between the two shapes for each head.

Feature representation updates. The cross-attention matrix is used to update the point representations for the query shape \mathcal{S}_m :

$$\mathbf{z}_{m,i}^{(h)} = \sum_{j=1}^{P_n} \mathbf{A}_{m,n}^{(h)}[i, j] \mathbf{W}_v^{(h)} \mathbf{x}_{n,j} \quad (5)$$

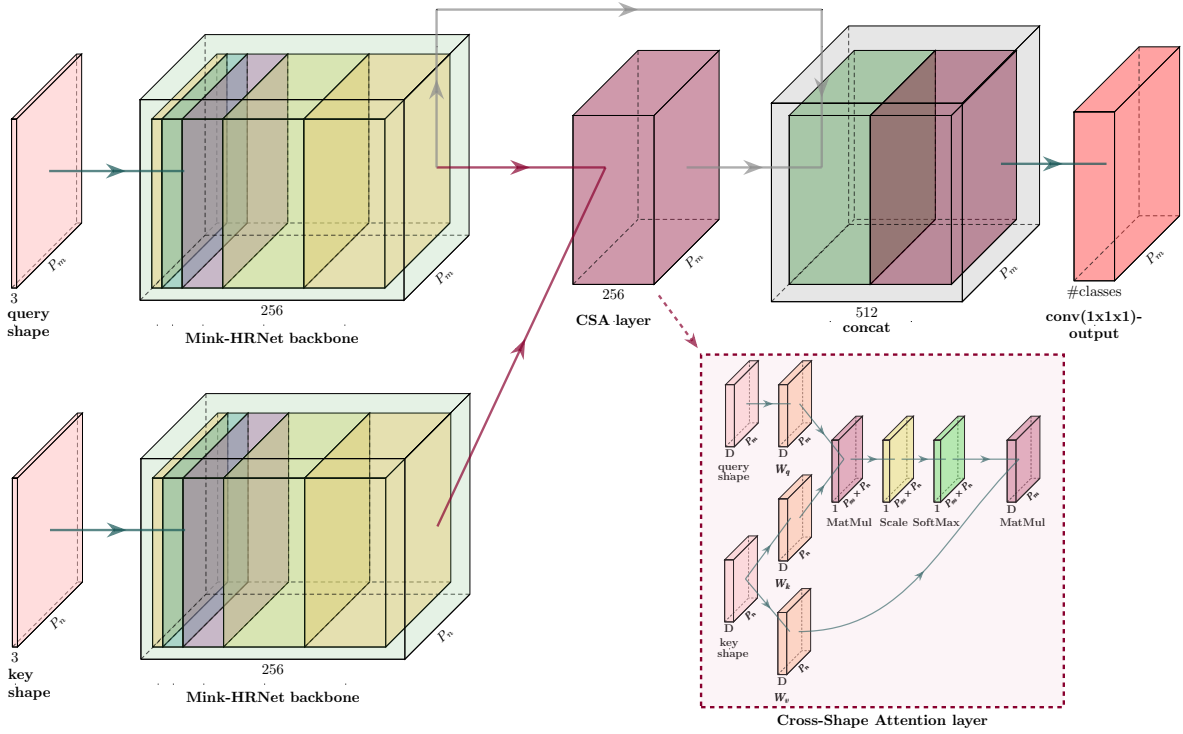


Figure 2. Our cross-shape network architecture: given an input test shape (“query shape”) represented as an input point set, we first extract multi-resolution point-wise features through a sparse tensor network backbone (“MinkNet-HRNet”). Then our proposed cross-attention layer, called CSA layer, propagates features extracted from another shape of the input shape collection (“key shape”) to the query shape such that their semantic segmentation becomes more synchronized. The output point-wise features of the CSA layer are concatenated with the original features of the query shape, then they are passed to a classification layer for semantic segmentation. Note that the illustrated CSA layer in the inlet figure uses only one head ($H = 1$).

The point-wise features are concatenated across all heads, then a linear transformation layer projects them back to D -dimensional space and are added back to the original point-wise features of the query shape:

$$\mathbf{x}'_{m,i} = \mathbf{x}_{m,i} + \mathbf{W}_d \cdot [\mathbf{z}_{m,i}^{(1)}, \mathbf{z}_{m,i}^{(2)}, \dots, \mathbf{z}_{m,i}^{(H)}] \quad (6)$$

where H is the number of heads (4 in our implementation), and \mathbf{W}_d is another linear transformation. The features are stacked into a matrix $\mathbf{X}'_m \in \mathcal{R}^{P_m \times D}$, followed by layer normalization [2].

Self-shape attention. The pairwise attention of Equation 4 and update operation of Equation 5 can also be applied to a pair that consists of the shape and itself. In this case, the CSA layer is equivalent to Self-Shape Attention (SSA), enabling long-range interactions between shape points within the same shape.

Cross-shape attention for multiple shapes. We can further generalize the cross-shape operation in order to handle

multiple shapes and also combine it with self-shape attention. Given a selected set of key shapes, our CSA layer outputs point representations for the query shape \mathcal{S}_m as follows:

$$\mathbf{X}'_m = \sum_{n \in \{\mathcal{C}(m), m\}} c(m, n) \mathbf{A}_{m,n} \mathbf{V}_n \quad (7)$$

where $\mathcal{C}(m)$ is a set of key shapes deemed compatible for cross-shape attention with shape \mathcal{S}_m and $c(m, n)$ is a learned pairwise compatibility function between the query shape \mathcal{S}_m and each key shape \mathcal{S}_n . The key idea of the above operation is to update point representations of the query shape \mathcal{S}_m as a weighted average of attention-modulated representations computed by using other key shapes as well as the shape itself. The compatibility function $c(m, n)$ assesses these weights that different shapes should have for cross-shape attention. It also implicitly provides the weight of self-shape attention when $\mathcal{S}_m = \mathcal{S}_n$.

Compatibility function. To compute the compatibility function, we first extract a global, D -dimensional vector representation \mathbf{y}_m and \mathbf{y}_n for the query shape \mathcal{S}_m and each

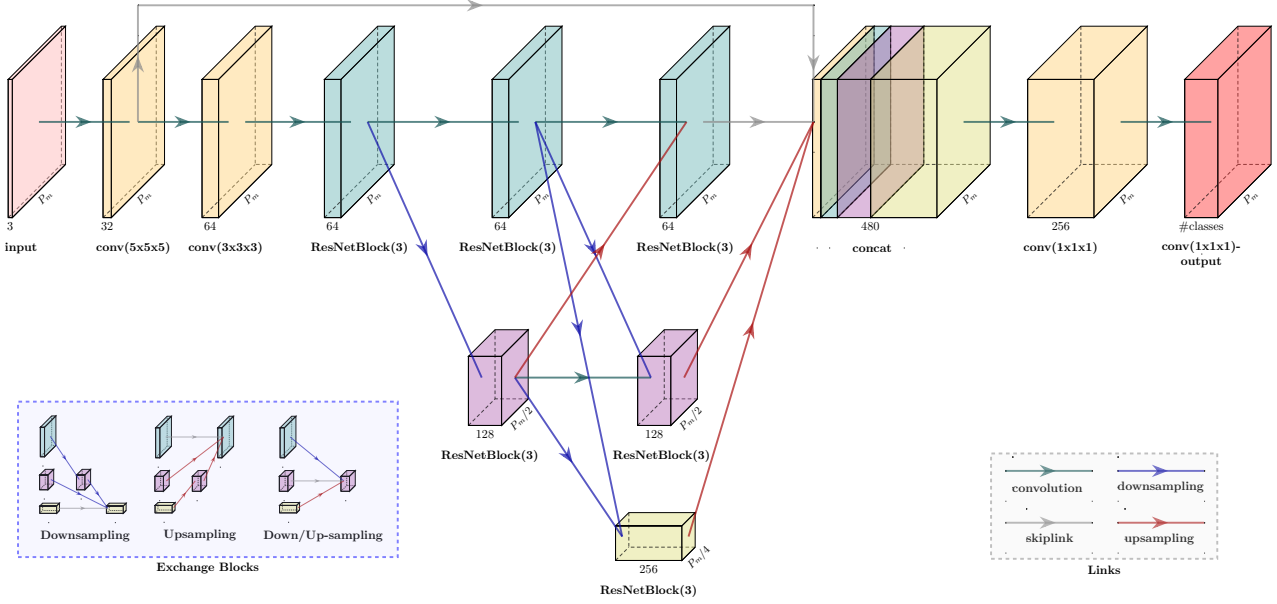


Figure 3. Our “Mink-HRNet” backbone consists of 3 multi-resolution branches. At each stage, branches exchange information either by downsampling and upsampling mechanisms or a mechanism that combines both (inlet figure on the bottom left).

key shape \mathcal{S}_n respectively through mean-pooling on their self-shape attention representations:

$$\mathbf{y}_m^{(SSA)} = \text{avg}_{\mathcal{S}_i} \mathbf{X}'_{m,i}{}^{(SSA)} = \text{avg}_i (\mathbf{A}_{m,m} \mathbf{V}_m) \quad (8)$$

$$\mathbf{y}_n^{(SSA)} = \text{avg}_{\mathcal{S}_i} \mathbf{X}'_{n,i}{}^{(SSA)} = \text{avg}_i (\mathbf{A}_{n,n} \mathbf{V}_n) \quad (9)$$

In this manner, the self-attention representations of both shapes provide cues for the compatibility between them expressed using their scaled dot product similarity [55]:

$$\begin{aligned} \mathbf{u}_m &= \mathbf{U}_q \mathbf{y}_m^{(SSA)} \\ \mathbf{u}_n &= \mathbf{U}_k \mathbf{y}_n^{(SSA)} \\ s(m, n) &= (\hat{\mathbf{u}}_m \cdot \hat{\mathbf{u}}_n^\top) / \sqrt{D} \end{aligned} \quad (10)$$

where \mathbf{U}_q and \mathbf{U}_k are learned $D \times D$ transformations for the query and key shape respectively, and $\hat{\mathbf{u}}_m = \mathbf{u}_m / \|\mathbf{u}_m\|$, $\hat{\mathbf{u}}_n = \mathbf{u}_n / \|\mathbf{u}_n\|$. The final compatibility function $c(m, n)$ is computed as a normalized measure using a softmax transformation of compatibilities of the shape m with all other shapes in the set $\mathcal{C}(m)$, including the self-compatibility:

$$c(m, n) = \frac{\exp(s(m, n))}{\sum_{n \in \{\mathcal{C}(m), m\}} \exp(s(m, n))} \quad (11)$$

3.2. Key shape retrieval

To perform cross-shape attention, we need to retrieve one or more key shapes for each query shape. One possibility is

to use the measure of Eq. 10 to evaluate the compatibility of the query shape with each candidate key shape from an input collection. However, we found that this compatibility is more appropriate for the particular task of weighting the contribution of each selected key shape for cross-shape attention, rather than retrieving key shapes themselves (see also supplementary material for additional discussion). We found that it is instead better to retrieve key shapes whose point-wise representations are on average more similar to the ones of the query shape. To achieve this, we perform the following steps:

(i) We compute the similarity between points of the query shape and the points of candidate key shapes in terms of cosine similarity of their SSA representations:

$$\mathbf{S}_{m,n} = \hat{\mathbf{X}}_m'^{(SSA)} \cdot (\hat{\mathbf{X}}_n'^{(SSA)})^\top \quad (12)$$

where $\mathbf{S}_{m,n} \in \mathcal{R}^{P_m \times P_n}$.

(ii) Then for each query point, we find its best matching candidate key shape point yielding the highest cosine similarity:

$$r_i(m, n) = \max_j \mathbf{S}_{m,n}[i, j] \quad (13)$$

(iii) Finally, we compute the average of these highest similarities across all query points:

$$r(m, n) = \text{avg}_i r_i(m, n) \quad (14)$$

The retrieval measure $r(m, n)$ is used to compare the query shape \mathcal{S}_n with candidate key shapes from a collection.

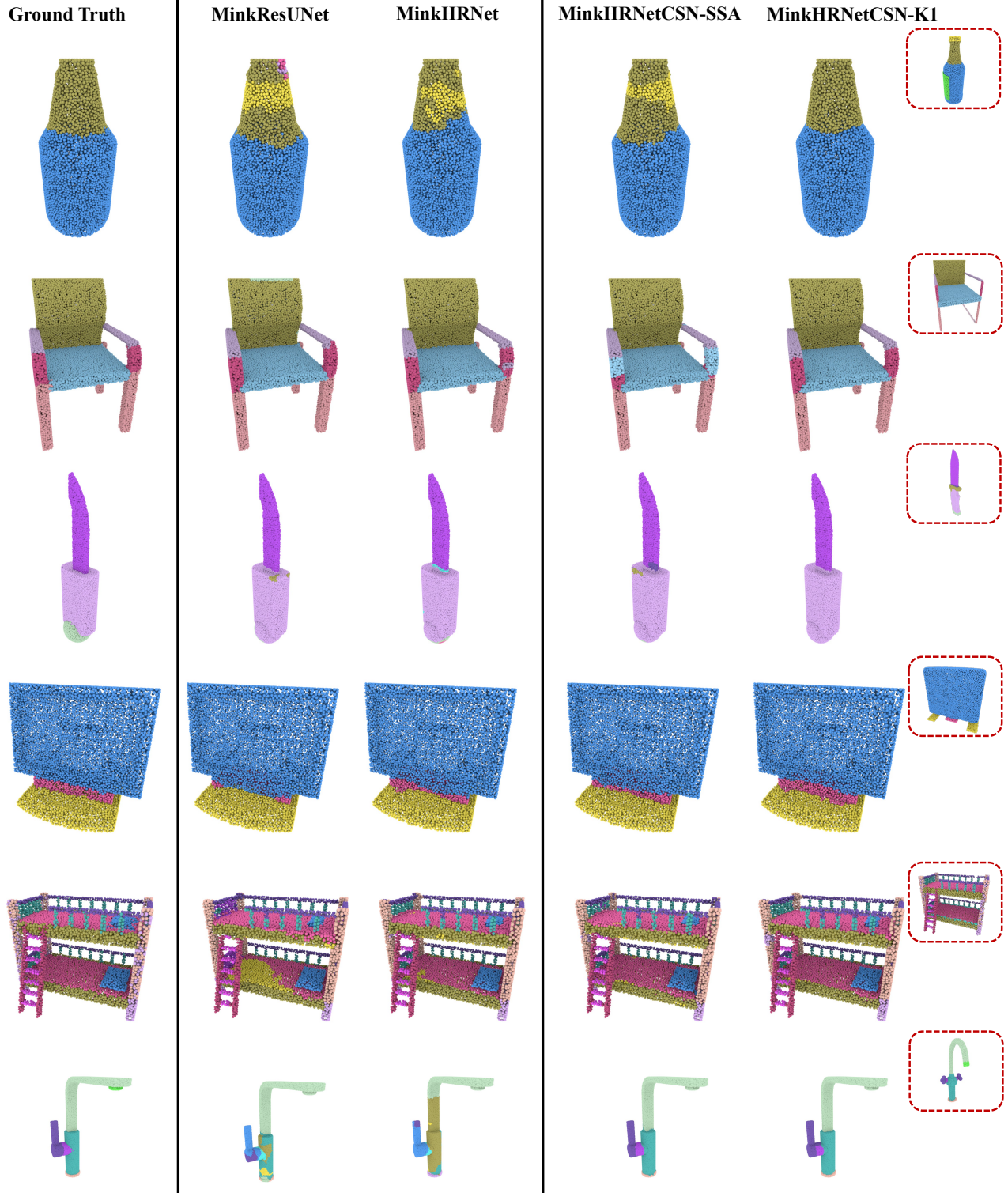


Figure 4. Qualitative comparisons for a few characteristic test shapes of PartNet between the original MinkowskiNet for 3D shape segmentation (“MinkResUNet”), our backbone (“MinkHRNet”), and CrossShapeNet (CSN) in case of using self-shape attention alone (“MinkHRNetCSN-SSA”) and using cross-shape attention with $K = 1$ key shape per query shape (“MinkHRNetCSN-K1”). The inlet images (red dotted box) show this key shape retrieved for each of the test shapes.

Category	Bed	Bott	Chai	Cloc	Dish	Disp	Door	Ear	Fauc	Knif	Lamp	Micr	Frid	Stor	Tabl	Tras	Vase	avg.	#cat.
Part IoU																			
PointNet++ [44]	30.3	41.4	39.2	41.6	50.1	80.7	32.6	38.4	52.4	34.1	25.3	48.5	36.4	40.5	33.9	46.7	49.8	42.5	0
ResGCN-28 [31]	35.9	49.3	41.1	33.8	56.2	81.0	31.1	45.8	52.8	44.5	23.1	51.8	34.9	47.2	33.6	50.8	54.2	45.1	0
PointCNN [33]	41.9	41.8	43.9	36.3	58.7	82.5	37.8	48.9	60.5	34.1	20.1	58.2	42.9	49.4	21.3	53.1	58.9	46.5	4
MinkResUNet (baseline)	39.4	44.2	42.3	35.4	57.8	82.4	33.9	45.8	57.8	46.7	25.0	53.7	40.5	45.0	35.7	50.6	58.8	46.8	0
MinkHRNet	41.8	46.0	43.3	36.1	60.5	82.3	39.3	49.5	58.0	42.6	25.6	57.0	40.2	46.3	37.4	51.9	59.0	48.0	1
MinkHRNetCSN-SSA	41.3	44.6	43.1	40.3	58.3	82.8	41.5	52.2	58.1	48.5	28.7	54.2	42.0	46.4	36.3	50.5	59.1	48.7	2
MinkHRNetCSN-K1	42.1	54.0	42.5	42.9	58.2	83.2	43.5	51.5	59.4	47.8	27.9	57.4	43.7	46.2	36.8	51.5	60.0	49.9	4
MinkHRNetCSN-K2	42.4	48.5	44.0	39.1	60.8	83.2	44.5	53.8	60.1	46.0	28.2	57.4	43.3	46.1	35.2	52.6	59.5	49.7	4
MinkHRNetCSN-K3	41.8	40.4	40.3	36.0	58.1	83.3	45.3	51.4	58.9	39.3	26.2	56.7	41.5	45.2	26.9	52.2	59.0	47.2	2
Shape IoU																			
PointNet++ [44]	25.1	61.0	49.6	46.1	52.5	81.0	48.0	56.1	60.4	49.1	46.0	54.3	50.7	50.6	47.0	54.7	75.1	53.4	2
PointCNN [33]	29.1	58.7	47.7	36.2	55.3	81.5	40.4	55.8	60.7	26.4	34.4	58.7	50.8	52.3	37.4	50.8	67.0	49.6	0
MinkResUNet (baseline)	28.5	56.7	46.9	49.6	56.8	82.4	47.6	53.1	63.3	44.6	38.6	58.4	54.7	50.1	43.6	48.4	75.8	52.9	0
MinkHRNet	29.9	59.7	49.1	47.2	58.5	82.4	51.5	55.9	64.9	45.6	38.6	62.0	54.1	51.8	44.7	49.6	80.1	54.4	2
MinkHRNetCSN-SSA	31.6	59.5	52.2	49.4	56.9	82.2	50.3	59.0	66.0	50.3	44.7	61.2	55.4	52.6	47.3	52.4	81.2	56.0	5
MinkHRNetCSN-K1	30.5	61.6	50.0	52.1	56.8	83.7	50.8	57.6	66.4	53.4	45.0	60.8	54.4	52.0	47.1	52.5	81.1	56.2	5
MinkHRNetCSN-K2	32.2	61.1	50.3	48.6	56.2	82.8	51.9	56.7	66.2	51.0	44.3	60.6	53.2	51.9	49.5	53.1	80.9	55.6	3
MinkHRNetCSN-K3	31.1	57.6	47.7	49.5	56.8	82.3	49.5	55.3	63.6	44.7	41.8	58.8	52.8	50.1	43.1	50.2	76.5	53.6	0

Table 1. Our evaluation on the fine-grained level of segmentation in PartNet categories. We report both the part IoU and shape IoU performance. In the last column, we report the number of categories that each method achieves the best quantitative results. We note that in ResGCN-28 [31], Shape IoU is not reported, thus we omit it for this measure.

3.3. Training

The input to our training procedure is a collection of point clouds with part annotations along with a smaller annotated collection used for hold-out validation. We first train our backbone including a layer that implements self-shape attention alone according to Eq. 3-6 (i.e., $\mathcal{S}_m = \mathcal{S}_n$ in this case). The resulting output features are passed to a softmax layer for semantic segmentation. The network is trained according to softmax loss. Based on the resulting SSA features, we construct a graph (Figure 1), where each training shape is connected with K shapes, deemed as “key” shapes, according to our retrieval measure of Eq. 14. One such graph is constructed for the training split, and another for the validation split. We then fine-tune our backbone and train a layer that implements our full cross-shape attention involving all K key shapes per training shape using the same loss. During training, we measure the performance of the network on the validation split, in terms of part IoU [40], and if it reaches a plateau state, we recalculate the K -neighborhood of each shape based on the updated features. We further fine-tune our backbone and CSA layer. This iteration of graph update and fine-tuning of our network is performed two times in our implementation.

3.4. Inference

During inference, we create a graph connecting each test shape with K training shapes retrieved by the measure of Eq. 14. We then perform a feed-forward pass through our backbone, CSA layer, and classification layer to assess the label probabilities for each test shape.

3.5. Architecture

We used a modified version of a sparse tensor network based on MinkowskiNet [9], as a backbone for extracting point-wise features, which serve as input to our CSA layer. We also experimented with a DGCNN backbone, yet the performance of this backbone was significantly lower than our sparse tensor network – see supplementary material for discussion of the DGCNN backbone. We here describe the details of the sparse tensor network architecture.

The architecture of our MinkowskiNet variant, called “MinkNetHRNet” is shown in Figure 3. We note that our variant performed better than the original MinkowskiNet for 3D segmentation [9], as discussed in our experiments. In a pre-processing step, we normalize the point clouds to a unit sphere and convert them to a sparse voxel grid (voxel size = 0.05). After two convolutional layers, the network branches into three stages inspired by the HRNet [57], a network that processes 2D images in a multi-resolution manner. In our case, the first stage consists of three residual blocks processing the sparse voxel grid in its original resolution. The second stage downsamples the voxel grid by a factor of 2 and processes it through two other residual blocks. The third stage further downsamples the voxel grid by a factor of 2 and processes it through another residual block. The multi-resolution features from the three stages are combined into one feature map through upsampling following [57]. The resulting feature map is further processed by a 1D convolutional block. The sparse voxel features are then mapped back to points as done in the original MinkowskiNet [9]. We also refer readers to our project page with source code for more details.

4. Results

We evaluated our CrossShapeNet for fine-grained shape segmentation both qualitatively and quantitatively. In the next paragraphs, we discuss the used dataset, evaluation metrics, and comparisons.

Dataset. We use the PartNet dataset [40] for training and evaluating our method according to its provided training, validation, and testing splits. Our evaluation focuses on the fine-grained level of semantic segmentation, which includes 17 out of the 24 object categories present in the PartNet dataset. We trained our network and competing variants separately for each object category.

Evaluation Metrics. For evaluating the performance of our method and variants, we used the standard part IoU and shape IoU metrics, as also proposed in the PartNet benchmark [40].

Competing methods. We first include comparisons with methods reporting their performance on PartNet. We then include a comparison with the original MinkowskiNet proposed in [9] for 3D shape segmentation (“MinkResUNet”). Most importantly, we compare our network with our backbone (“MinkHRNet”), since the main goal of our evaluation is to check whether the addition of the CSA layer yields better features than the ones produced by our raw backbone. In addition, we include a comparison with a variant of our architecture using exclusively self-shape attention (“MinkHRNetCSN-SSA”). Our CSA layer is tested in the variants “MinkHRNetCSN-K1”, “MinkHRNetCSN-K2”, and “MinkHRNetCSN-K3”, where we use $K = 1, 2, 3$ key shapes per query shape.

Quantitative Results. Table 1 reports the performance of all competing methods. We first observe that our backbone variant “MinkHRNet” improves over the original “MinkResUNet” used in [9], yielding an improvement of 1.2% in Part IoU and 1.5% in Shape IoU. Our variant based on self-shape attention alone further improves our backbone by 0.7% in Part IoU and 1.6% in Shape IoU. Our CrossShapeNet with $K = 1$ (“MinkHRNetCSN-K1”) offers the best performance on average by improving Part IoU by another 1.2% with respect to using self-shape attention alone, while having almost similar shape IoU performance (+0.2%). *Compared to our backbone, “MinkHRNetCSN-K1” offers a noticeable improvement of 1.9% in terms of Part IoU, and also 1.8% in terms of Shape IoU.*

When using $K = 2$ key shapes in cross-shape attention, the performance drops slightly (−0.2% in Part IoU on average), yet interestingly, this variant still achieves better Part

IoU performance compared to using $K = 1$ for 8 out of the 17 classes.

For two of the PartNet classes (“Door”, “Display”), the optimal number of key shapes is $K = 3$. In general, the optimal number of key shapes ranges from $K = 1$ to $K = 3$ depending on the shape class. In terms of average Part IoU and Shape IoU across all classes, best performance is achieved with $K = 1$. The performance drop for higher K is due to the issue that the chance of retrieving shapes incompatible to the query shape is increased with larger numbers of retrieved key shapes.

Qualitative Results. Figure 4 shows qualitative comparisons between our method based on cross-shape attention with $K = 1$, self-shape attention, our backbone, and the original MinkowskiNet. Our backbone often improves the labeling relative to the original MinkowskiNet (e.g., see bed mattress, or monitor base). Our cross-shape attention tends to further improve upon fine-grained details in the segmentation e.g., see the top of the bottle, the armrests in the chair, and the bottom of the blade, pushing the segmentation to be more consistent with the retrieved key shape shown in the inlet images.

Number of parameters. Our CSA layer adds a relatively small overhead in terms of number of parameters compared to our backbone: the backbone has 24.8M parameters, while the CSA layer adds 0.4M parameters.

Computation. Training with our CSA layer for $K = 1$ takes 105 hours on a NVidia V100 for the largest PartNet category (3.75 times more compared to training the backbone alone) due to the need of the iterative graph construction and fine-tuning discussed in Section 3.3. The inference time per test shape increases linearly with the size of the input collection used for retrieval. In our experiments, testing time ranges from 0.7 seconds (“Dish” class having the smallest number of shapes in PartNet) to 7.8 seconds (“Table” class having the largest number of shapes).

5. Conclusion

We presented a method that enables interaction of point-wise features across different shapes in a collection. The interaction is mediated through a new cross-shape attention mechanism. Our experiments show improvements of this interaction in the case of fine-grained shape segmentation.

Limitations. First, we note that the performance increase comes with a higher computational cost at training and test time. It would be interesting to explore if further performance gains can be achieved through self-supervised pre-training of point correspondences as done in e.g., Point-

Contrast [68] that could in turn guide the attention mechanism. Sparsifying the attention mechanism [8] would be beneficial in this case to handle the quadratic computational complexity of our current attention mechanism. Accelerating the key shape retrieval mechanism would also be useful to further decrease the test time. Another future research direction is to explore how to generalize the cross-shape attention mechanism from single shapes to entire scenes.

References

- [1] Matan Atzmon, Haggai Maron, and Yaron Lipman. Point Convolutional Neural Networks by Extension Operators. *ACM Trans. on Graphics*, 37(4), 2018. 2
- [2] Jimmy Ba, Jamie Ryan Kiros, and Geoffrey E. Hinton. Layer Normalization. *arXiv preprint arXiv:1607.06450*, 2016. 4, 12
- [3] Davide Boscaini, Jonathan Masci, Simone Melzi, Michael M Bronstein, Umberto Castellani, and Pierre Vandergheynst. Learning class-specific descriptors for deformable shapes using localized spectral convolutional networks. *Computer Graphics Forum*, 34(5), 2015. 2
- [4] Davide Boscaini, Jonathan Masci, Emanuele Rodolà, and Michael Bronstein. Learning shape correspondence with anisotropic convolutional neural networks. In *Proc. NeurIPS*, 2016. 2
- [5] Anh-Quan Cao, Gilles Puy, Alexandre Boulch, and Renaud Marlet. PCAM: Product of Cross-Attention Matrices for Rigid Registration of Point Clouds. In *Proc. ICCV*, 2021. 2
- [6] Yue Cao, Jiarui Xu, Stephen Lin, Fangyun Wei, and Han Hu. GCNet: Non-local networks meet squeeze-excitation networks and beyond. In *Proc. CVPR Workshops*, 2019. 2
- [7] Chun-Fu (Richard) Chen, Quanfu Fan, and Rameswar Panda. CrossViT: Cross-Attention Multi-Scale Vision Transformer for Image Classification. In *Proc. ICCV*, 2021. 3
- [8] Rewon Child, Scott Gray, Alec Radford, and Ilya Sutskever. Generating Long Sequences with Sparse Transformers. *arXiv preprint arXiv:1904.10509*, 2019. 9
- [9] Christopher Choy, JunYoung Gwak, and Silvio Savarese. 4D Spatio-Temporal ConvNets: Minkowski Convolutional Neural Networks. In *Proc. CVPR*, 2019. 1, 3, 7, 8
- [10] NVIDIA Corporation Chris Choy. *Minkowski Engine*, 2020. 12
- [11] Angela Dai, Angel X Chang, Manolis Savva, Maciej Halber, Thomas Funkhouser, and Matthias Nießner. ScanNet: Richly-annotated 3d reconstructions of indoor scenes. In *Proc. CVPR*, 2017. 2
- [12] Carl Doersch, Ankush Gupta, and Andrew Zisserman. Crosstransformers: spatially-aware few-shot transfer. In *Proc. NeurIPS*, 2020. 3
- [13] Nico Engel, Vasileios Belagiannis, and Klaus Dietmayer. Point transformer. *IEEE Access*, 9, 2021. 2
- [14] Fabian Groh, Patrick Wieschollek, and Hendrik P. A. Lensch. Flex-Convolution (Million-Scale Point-Cloud Learning Beyond Grid-Worlds). In *Proc. ACCV*, 2018. 2
- [15] Meng-Hao Guo, Jun-Xiong Cai, Zheng-Ning Liu, Tai-Jiang Mu, Ralph R Martin, and Shi-Min Hu. Pct: Point cloud transformer. *Computational Visual Media*, 7(2), 2021. 2
- [16] Wenkai Han, Chenglu Wen, Cheng Wang, Xin Li, and Qing Li. Point2Node: Correlation Learning of Dynamic-Node for Point Cloud Feature Modeling. *arXiv preprint arXiv:1912.10775*, 2019. 2
- [17] Pedro Hermosilla, Tobias Ritschel, Pere-Pau Vázquez, Àlvar Vinacua, and Timo Ropinski. Monte Carlo Convolution for Learning on Non-Uniformly Sampled Point Clouds. *ACM Trans. on Graphics*, 37(6), 2018. 2
- [18] Ruibing Hou, Hong Chang, MA Bingpeng, Shiguang Shan, and Xilin Chen. Cross Attention Network for Few-shot Classification. In *Proc. NeurIPS*, 2019. 2
- [19] Binh-Son Hua, Minh-Khoi Tran, and Sai-Kit Yeung. Point-wise convolutional neural networks. In *Proc. CVPR*, 2018. 2
- [20] Haibin Huang, Evangelos Kalogerakis, Siddhartha Chaudhuri, Duygu Ceylan, Vladimir G. Kim, and Ersin Yumer. Learning Local Shape Descriptors from Part Correspondences with Multiview Convolutional Networks. *ACM Trans. on Graphics*, 37(1), 2017. 2
- [21] Zilong Huang, Xinggang Wang, Lichao Huang, Chang Huang, Yunchao Wei, and Wenyu Liu. CCNet: Criss-cross attention for semantic segmentation. In *Proc. CVPR*, 2019. 2
- [22] Sergey Ioffe and Christian Szegedy. Batch Normalization: Accelerating Deep Network Training by Reducing Internal Covariate Shift. In *Proc. ICML*, 2015. 12
- [23] Li Jiang, Hengshuang Zhao, Shu Liu, Xiaoyong Shen, Chi-Wing Fu, and Jiaya Jia. Hierarchical point-edge interaction network for point cloud semantic segmentation. In *Proc. CVPR*, 2019. 2
- [24] Evangelos Kalogerakis, Melinos Averkiou, Subhansu Maji, and Siddhartha Chaudhuri. 3d shape segmentation with projective convolutional networks. In *Proc. CVPR*, 2017. 2
- [25] Roman Klokov and Victor Lempitsky. Escape from cells: Deep KD-networks for the recognition of 3d point cloud models. In *Proc. CVPR*, 2017. 2
- [26] Artem Komarichev, Zichun Zhong, and Jing Hua. A-CNN: Annularly convolutional neural networks on point clouds. In *Proc. CVPR*, 2019. 2
- [27] Shiyi Lan, Ruichi Yu, Gang Yu, and Larry S Davis. Modeling local geometric structure of 3D point clouds using Geo-CNN. In *Proc. CVPR*, 2019. 2
- [28] Loic Landrieu and Mohamed Boussaha. Point cloud over-segmentation with graph-structured deep metric learning. In *Proc. CVPR*, 2019. 2
- [29] Eric-Tuan Le, Iasonas Kokkinos, and Niloy J Mitra. Going Deeper with Point Networks. *arXiv preprint arXiv:1907.00960*, 2019. 2
- [30] Kuang-Huei Lee, Xi Chen, Gang Hua, Houdong Hu, and Xiaodong He. Stacked cross attention for image-text matching. In *Proc. ECCV*, 2018. 2
- [31] Guohao Li, Matthias Müller, Guocheng Qian, Itzel Carolina Delgadillo Perez, Abdullellah Abualshour, Ali Kassem Thabet, and Bernard Ghanem. Deepgcns: Making gcns go

- as deep as cnns. *IEEE Trans. Pat. Ana. & Mach. Int.*, 2021. [2, 7](#)
- [32] Jiaxin Li, Ben Chen, and Gim Lee. SO-Net: Self-Organizing Network for Point Cloud Analysis. In *Proc. CVPR*, 2018. [2](#)
- [33] Yangyan Li, Rui Bu, Mingchao Sun, Wei Wu, Xinhao Di, and Baoquan Chen. PointCNN: Convolution On X-Transformed Points. In *Proc. NeurIPS*, 2018. [2, 7](#)
- [34] Yongcheng Liu, Bin Fan, Gaofeng Meng, Jiwen Lu, Shiming Xiang, and Chunhong Pan. DensePoint: Learning Densely Contextual Representation for Efficient Point Cloud Processing. In *Proc. ICCV*, 2019. [2](#)
- [35] Yongcheng Liu, Bin Fan, Shiming Xiang, and Chunhong Pan. Relation-shape convolutional neural network for point cloud analysis. In *Proc. CVPR*, 2019. [2](#)
- [36] Zhijian Liu, Haotian Tang, Yujun Lin, and Song Han. Point-Voxel CNN for efficient 3D deep learning. In *Proc. NeurIPS*, 2019. [2](#)
- [37] Daniel Maturana and Sebastian Scherer. Voxnet: A 3D convolutional neural network for real-time object recognition. In *Proc. IROS*, 2015. [2](#)
- [38] Kirill Mazur and Victor Lempitsky. Cloud Transformers: A Universal Approach to Point Cloud Processing Tasks. In *Proc. ICCV*, 2021. [2](#)
- [39] Kaichun Mo, Shilin Zhu, Angel X Chang, Li Yi, Subarna Tripathi, Leonidas J Guibas, and Hao Su. PartNet: A Large-scale Benchmark for Fine-grained and Hierarchical Part-level 3D Object Understanding. In *Proc. CVPR*, 2019. [1](#)
- [40] Kaichun Mo, Shilin Zhu, Angel X. Chang, Li Yi, Subarna Tripathi, Leonidas J. Guibas, and Hao Su. PartNet: A Large-Scale Benchmark for Fine-Grained and Hierarchical Part-Level 3D Object Understanding. In *Proc. CVPR*, 2019. [7, 8, 11](#)
- [41] Federico Monti, Davide Boscaini, Jonathan Masci, Emanuele Rodola, Jan Svoboda, and Michael M Bronstein. Geometric deep learning on graphs and manifolds using mixture model cnns. In *Proc. CVPR*, 2017. [2](#)
- [42] Charles R. Qi, Hao Su, Kaichun Mo, and Leonidas Guibas. PointNet: Deep Learning on Point Sets for 3D Classification and Segmentation. In *Proc. CVPR*, 2017. [2](#)
- [43] Charles R Qi, Hao Su, Matthias Nießner, Angela Dai, Mengyuan Yan, and Leonidas J Guibas. Volumetric and multi-view cnns for object classification on 3d data. In *Proc. CVPR*, 2016. [2](#)
- [44] Charles R. Qi, Li Yi, Hao Su, and Leonidas J. Guibas. PointNet++: Deep Hierarchical Feature Learning on Point Sets in a Metric Space. In *Proc. NeurIPS*, 2017. [2, 7](#)
- [45] Dario Reithage, Johanna Wald, Jurgen Sturm, Nassir Navab, and Federico Tombari. Fully-convolutional point networks for large-scale point clouds. In *Proc. ECCV*, 2018. [2](#)
- [46] Gernot Riegler, Ali Osman Ulusoy, and Andreas Geiger. OctNet: Learning Deep 3D Representations at High Resolutions. In *CVPR*, 2017. [2](#)
- [47] Sebastian Ruder. An overview of gradient descent optimization algorithms. *arXiv preprint arXiv:1609.04747*, 2016. [11](#)
- [48] Paul-Edouard Sarlin, Daniel DeTone, Tomasz Malisiewicz, and Andrew Rabinovich. SuperGlue: Learning Feature Matching with Graph Neural Networks. *arXiv preprint arXiv:1911.11763*, 2019. [2](#)
- [49] Yiru Shen, Chen Feng, Yaoqing Yang, and Dong Tian. Mining Point Cloud Local Structures by Kernel Correlation and Graph Pooling. In *Proc. CVPR*, 2018. [2](#)
- [50] Shaoshuai Shi, Xiaogang Wang, and Hongsheng Li. PointRCNN: 3D Object Proposal Generation and Detection From Point Cloud. In *Proc. CVPR*, 2019. [2](#)
- [51] Nitish Srivastava, Hanlin Goh, and Ruslan Salakhutdinov. Geometric Capsule Autoencoders for 3D Point Clouds. *arXiv preprint arXiv:1912.03310*, 2019. [2](#)
- [52] Hang Su, Varun Jampani, Deqing Sun, Subhransu Maji, Evangelos Kalogerakis, Ming-Hsuan Yang, and Jan Kautz. SPLATNet: Sparse Lattice Networks for Point Cloud Processing. In *Proc. CVPR*, 2018. [2](#)
- [53] Hang Su, Subhransu Maji, Evangelos Kalogerakis, and Erik Learned-Miller. Multi-view convolutional neural networks for 3d shape recognition. In *Proc. ICCV*, 2015. [2](#)
- [54] Hugues Thomas, Charles R Qi, Jean-Emmanuel Deschaud, Beatriz Marcotegeui, François Goulette, and Leonidas J Guibas. KPConv: Flexible and deformable convolution for point clouds. In *Proc. CVPR*, 2019. [2](#)
- [55] Ashish Vaswani, Noam Shazeer, Niki Parmar, Jakob Uszkoreit, Llion Jones, Aidan N Gomez, L ukasz Kaiser, and Illia Polosukhin. Attention is All you Need. In *Proc. NeurIPS*, 2017. [3, 5](#)
- [56] Chu Wang, Babak Samari, and Kaleem Siddiqi. Local Spectral Graph Convolution for Point Set Feature Learning. *arXiv preprint arXiv:1803.05827*, 2018. [2](#)
- [57] Jingdong Wang, Ke Sun, Tianheng Cheng, Borui Jiang, Chaorui Deng, Yang Zhao, Dong Liu, Yadong Mu, Mingkui Tan, Xinggang Wang, Wenyu Liu, and Bin Xiao. Deep High-Resolution Representation Learning for Visual Recognition. *IEEE Trans. Pat. Ana. & Mach. Int.*, 43(10), 2021. [1, 7, 11](#)
- [58] L. Wang, Y. Huang, Y. Hou, S. Zhang, and J. Shan. Graph Attention Convolution for Point Cloud Semantic Segmentation. In *Proc. CVPR*, 2019. [2](#)
- [59] Peng-Shuai Wang, Yang Liu, Yu-Xiao Guo, Chun-Yu Sun, and Xin Tong. O-CNN: Octree-based Convolutional Neural Networks for 3D Shape Analysis. *ACM Trans. on Graphics*, 36(4), 2017. [2](#)
- [60] Peng-Shuai Wang, Chun-Yu Sun, Yang Liu, and Xin Tong. Adaptive O-CNN: A Patch-based Deep Representation of 3D Shapes. *ACM Trans. on Graphics*, 37(6), 2018. [2](#)
- [61] Shenlong Wang, Simon Suo, Wei-Chiu Ma, Andrei Pokrovsky, and Raquel Urtasun. Deep parametric continuous convolutional neural networks. In *Proc. CVPR*, 2018. [2](#)
- [62] Xiaolong Wang, Ross Girshick, Abhinav Gupta, and Kaiming He. Non-local neural networks. In *Proc. CVPR*, 2018. [2](#)
- [63] Yue Wang and Justin M. Solomon. Deep Closest Point: Learning Representations for Point Cloud Registration. In *Proc. ICCV*, 2019. [2](#)
- [64] Yue Wang, Yongbin Sun, Ziwei Liu, Sanjay E. Sarma, Michael M. Bronstein, and Justin M. Solomon. Dynamic Graph CNN for Learning on Point Clouds. *ACM Trans. on Graphics*, 38(5), 2019. [2, 14](#)

- [65] Wenxuan Wu, Zhongang Qi, and Li Fuxin. Pointconv: Deep convolutional networks on 3d point clouds. In *Proc. CVPR*, 2019. 2
- [66] Zhirong Wu, Shuran Song, Aditya Khosla, Fisher Yu, Linguang Zhang, Xiaoou Tang, and Jianxiong Xiao. 3D shapenets: A deep representation for volumetric shapes. In *Proc. CVPR*, 2015. 2
- [67] Peng Xiang, Xin Wen, Yu-Shen Liu, Yan-Pei Cao, Pengfei Wan, Wen Zheng, and Zhizhong Han. SnowflakeNet: Point Cloud Completion by Snowflake Point Deconvolution With Skip-Transformer. In *Proc. ICCV*, 2021. 2
- [68] Saining Xie, Jiatao Gu, Demi Guo, Charles R. Qi, Leonidas Guibas, and Or Litany. PointContrast: Unsupervised Pre-training for 3D Point Cloud Understanding. In *Proc. ECCV*, 2020. 9
- [69] Saining Xie, Sainan Liu, Zeyu Chen, and Zhuowen Tu. Attentional shapecontextnet for point cloud recognition. In *Proc. CVPR*, 2018. 2
- [70] Qiangeng Xu, Xudong Sun, Cho ying Wu, Panqu Wang, and Ulrich Neumann. Grid-GCN for Fast and Scalable Point Cloud Learning. *arXiv preprint arXiv:1912.02984*, 2019. 2
- [71] Yifan Xu, Tianqi Fan, Mingye Xu, Long Zeng, and Yu Qiao. SpiderCNN: Deep Learning on Point Sets with Parameterized Convolutional Filters. *arXiv preprint arXiv:1803.11527*, 2018. 2
- [72] Li Yi, Hao Su, Xingwen Guo, and Leonidas J Guibas. Sync-SpecCNN: Synchronized spectral cnn for 3d shape segmentation. In *Proc. CVPR*, 2017. 2
- [73] Shi Yunxiao, Fang Haoyu, Zhu Jing, and Fang Yi. Pairwise Attention Encoding for Point Cloud Feature Learning. In *Proc. 3DV*, 2019. 2
- [74] Kuangen Zhang, Ming Hao, Jing Wang, Clarence W de Silva, and Chenglong Fu. Linked Dynamic Graph CNN: Learning on point cloud via linking hierarchical features. *arXiv preprint arXiv:1904.10014*, 2019. 2
- [75] Hengshuang Zhao, Li Jiang, Jiaya Jia, Philip HS Torr, and Vladlen Koltun. Point transformer. In *Proc. ICCV*, 2021. 2

– Supplementary Material –

Appendix A: MinkHRNetCSN details

Architecture details. In Table 2 we describe the overall Cross-Shape Network architecture for $K = 1$ key shapes per query shape, based on the HRNet [57] backbone (“MinkHRNetCSN-K1”). For $K = 2, 3$ and SSA variants, we use the same architecture. First, for an input query-key pair of shapes $\mathcal{S}_m \in \mathcal{R}^{P_m \times 3}$ and $\mathcal{S}_n \in \mathcal{R}^{P_n \times 3}$, point-wise features \mathbf{X}_m and \mathbf{X}_n are extracted using the “MinkHRNet” backbone (Layers 2 and 3). For each set of point features their self-shape attention representations are calculated via the *Cross-Shape Attention* layer (Layers 4 and 5). The query shape point self-shape attention representations are then aggregated into a global feature using mean-pooling and undergo two separate linear transformations (*Linear-Q* and *Linear-K* in Layers 6 and 7, respectively).

Leveraging these, the self-shape similarity is computed, using the *scaled dot product* (Layer 9). For the key shape point self-shape attention representations, we use only the *Linear-K* transformation on the key shape’s global feature (Layer 8), and calculate the query-key similarity (Layer 10). The compatibility for the cross-shape attention is computed as the softmax transformation of these two similarity measures (Layer 11). The cross-shape point representations of the query shape, propagating point features from the key shape, are extracted by our CSA module in Layer 12. The self-shape (Layer 4) and cross-shape (Layer 12) point representations are combined together, weighted by the pairwise compatibility, resulting in the cross-shape attention representations \mathbf{X}'_m (Layer 13). Finally, part label probabilities are extracted per point, through a $1 \times 1 \times 1$ convolution and a softmax transformation (Layer 14), based on the concatenation of the query shape’s backbone representations \mathbf{X}_m and cross-shape attention representations \mathbf{X}'_m .

The architecture of our backbone network, “MinkHRNet”, is described in Table 3. Based on an input shape, our backbone first extracts point representations through two consecutive convolutions (Layers 2-5). Then, three multi-resolution branches are deployed. The first branch, called *High-ResNetBlock* (Layers 6, 8 and 15), operates on the input shape’s resolution, while the other two, *Mid-ResNetBlock* (Layers 9 and 16) and *Low-ResNetBlock* (Layer 17), downsample the shape’s resolution by a factor of 2 and 4, respectively. In addition, feature representations are exchanged between these branches, through downsampling and upsampling modules (Layers 7, 10-14). The point representations of the two low-resolution branches are upsampled to the original resolution (Layers 18-20) and by concatenating them with point features of the high-resolution branch, point representations are extracted for the input shape, through a full-connected layer (Layers 21 and 22).

The *Cross-Shape Attention* (CSA), *Downsampling* and *Upsampling* layers, along with *Residual Basic Block* are described in more detail in Table 4.

Implementation details. We train our CSN architecture for each object category of PartNet [40] separately, using the standard cross entropy loss, for 200 epochs. We set the batch size equal to 8 for all variants (SSA, K=1,2,3). For optimization we use the SGD optimizer [47] with a learning rate of 0.5 and momentum = 0.9. We scale learning rate by a factor of 0.5, whenever the loss of the hold-out validation split saturates (patience = 10 epochs, cooldown = 10 epochs). For updating the shape graph for the training and validation split, we measure the performance of the validation split in terms of Part IoU. If it reaches a saturation point (patience = 10 epochs, cooldown = 5 epochs), we load the best model up to that moment, based on Part

Cross-shape network architecture		\leftarrow CSN(<i>query</i> \mathcal{S}_m , <i>key</i> \mathcal{S}_n , #classes K)
Index	Layer	Out
1	<i>Input</i> : $\mathcal{S}_m, \mathcal{S}_n$	$P_m \times 3, P_n \times 3$
2	<i>Mink-HRNet</i> (\mathcal{S}_m , 3, 256)	$P_m \times 256$ - query point repr.
3	<i>Mink-HRNet</i> (\mathcal{S}_n , 3, 256)	$P_n \times 256$ - key point repr.
4	CSA(Out(2), Out(2), 256, 4)	$P_m \times 256$ - query SSA repr.
5	CSA(Out(3), Out(3), 256, 4)	$P_n \times 256$ - key SSA repr.
6	<i>Linear-Q</i> (<i>avg-pool</i> (Out(4)), 256, 256)	1×256 - query global repr.
7	<i>Linear-K</i> (<i>avg-pool</i> (Out(4)), 256, 256)	1×256 - query global repr.
8	<i>Linear-K</i> (<i>avg-pool</i> (Out(5)), 256, 256)	1×256 - key global repr.
9	<i>ScaledDotProduct</i> (Out(6), Out(7))	1×1 - query-query similarity
10	<i>ScaledDotProduct</i> (Out(6), Out(8))	1×1 - query-key similarity
11	<i>Softmax</i> (Out(9), Out(10))	2×1 - compatibility
12	CSA(Out(2), Out(3), 256, 4)	$P_m \times 256$ - query CSA repr.
13	Out(4) * <i>compatibility</i> [0] + Out(12) * <i>compatibility</i> [1]	$P_m \times 256$ - cross-shape attention
14	<i>Softmax</i> (<i>Conv</i> (<i>ConCat</i> (Out(2), Out(13)), 512, K))	$P_m \times K$ - per-point part label probabilities

Table 2. Cross-shape network architecture for $K = 1$ key shapes per query shape.

Mink-HRNet backbone		\leftarrow Mink-HRNet(<i>shape repr.</i> \mathbf{X}_m , <i>in-feat</i> D_{in} , <i>out-feat</i> D_{out})
Index	Layer	Out
1	<i>Input</i> : \mathbf{X}_m	$P_m \times D_{in}$
2	<i>Conv</i> (\mathbf{X}_m , D_{in} , 32)	$P_m \times 32$
3	<i>ReLU</i> (<i>BatchNorm</i> (Out(2)))	$P_m \times 32$
4	<i>Conv</i> (Out(3), 32, 64)	$P_m \times 64$
5	<i>ReLU</i> (<i>BatchNorm</i> (Out(4)))	$P_m \times 64$
6	<i>High-ResNetBlock</i> ($3 \times$ <i>BasicBlock</i> (Out(5), 64))	$P_m \times 64$
7	<i>Downsampling</i> (Out(6), 64, 128)	$P_m/2 \times 128$
8	<i>High-ResNetBlock</i> ($3 \times$ <i>BasicBlock</i> (Out(6), 64))	$P_m \times 64$
9	<i>Mid-ResNetBlock</i> ($3 \times$ <i>BasicBlock</i> (<i>ReLU</i> (Out(7)), 128))	$P_m/2 \times 128$
10	<i>Downsampling</i> (Out(8), 64, 128)	$P_m/2 \times 128$
11	<i>ReLU</i> (<i>Downsampling</i> (Out(8), 64, 128))	$P_m/2 \times 128$
12	<i>Downsampling</i> (Out(11), 128, 256)	$P_m/4 \times 256$
13	<i>Upsampling</i> (Out(9), 128, 64)	$P_m \times 64$
14	<i>Downsampling</i> (Out(9), 128, 256)	$P_m/4 \times 256$
15	<i>High-ResNetBlock</i> ($3 \times$ <i>BasicBlock</i> (<i>ReLU</i> (Out(8)+Out(13)), 64))	$P_m \times 64$
16	<i>Mid-ResNetBlock</i> ($3 \times$ <i>BasicBlock</i> (<i>ReLU</i> (Out(9) + Out(10)), 128))	$P_m/2 \times 128$
17	<i>Low-ResNetBlock</i> ($3 \times$ <i>BasicBlock</i> (<i>ReLU</i> (Out(12) + Out(14)), 256))	$P_m/4 \times 256$
18	<i>ReLU</i> (<i>Upsampling</i> (Out(16), 128, 128))	$P_m \times 128$
19	<i>ReLU</i> (<i>Upsampling</i> (Out(17), 256, 256))	$P_m/2 \times 256$
20	<i>ReLU</i> (<i>Upsampling</i> (Out(19), 256, 256))	$P_m \times 256$
21	<i>Conv</i> (<i>ConCat</i> (Out(3), Out(15), Out(18), Out(20)), 480, D_{out})	$P_m \times D_{out}$
22	<i>ReLU</i> (<i>BatchNorm</i> (Out(21)))	$P_m \times D_{out}$

Table 3. Mink-HRNet backbone architecture. High, mid and low-resolution ResNet blocks consist of 3 consecutive residual basic blocks, each. Point representations are exchanged between multi-resolution branches via downsampling and upsampling layers (see Table 4 for a more detailed description of their architecture). The convolution kernel of Layer 2 is of size $5 \times 5 \times 5$, in order to increase its receptive field, while for Layer 4 is of size $3 \times 3 \times 3$. For Layer 21 we used a kernel of $1 \times 1 \times 1$, since this acts as a fully-connected layer.

IoU performance, and update the graph for both splits. The graph is updated twice throughout our training procedure. For all layers we use batch normalization [22] with momentum = 0.02, except for the CSA module, where the layer normalization [2] is adopted. All networks and submodules were implemented using the MinkowskiEngine library [10].

Appendix B: Key shape retrieval

Here we evaluate the performance of our “MinkHRNetCSN-K1” variant for two key shape retrieval measures (see Section 3.2 in the main paper). The first relies on the point-wise representations between

Cross-Shape Attention Layer		$\leftarrow \text{CSA}(\text{query } \mathbf{X}_m, \text{key } \mathbf{X}_n, \text{\#feats } D, \text{\#heads } H)$
Index	Layer	Out
1	<i>Input: $\mathbf{X}_m, \mathbf{X}_n$</i>	$P_m \times D, P_n \times D$
2	$H \times \text{Linear-}Q(\mathbf{X}_m, D, \lfloor D/H \rfloor)$	$P_m \times H \times D'$
3	$H \times \text{Linear-}K(\mathbf{X}_n, D, \lfloor D/H \rfloor)$	$P_n \times H \times D'$
4	$H \times \text{Linear-}V(\mathbf{X}_n, D, \lfloor D/H \rfloor)$	$P_n \times H \times D'$
5	<i>Attention</i> (Out(2), Out(3))	$H \times P_m \times P_n$
6	<i>MatMul</i> (Out(5), Out(4))	$P_m \times H \times D'$
7	<i>Linear</i> (Concat(Out(6)), D, D)	$P_m \times D$
8	<i>LayerNorm</i> ($\mathbf{X}_m + \text{Out}(7)$)	$P_m \times D$
Downsampling Layer		$\leftarrow \text{Downsampling}(\text{shape repr. } \mathbf{X}_m, \text{in-feat } D_{in}, \text{out-feat } D_{out})$
1	<i>Input: \mathbf{X}_m</i>	$P_m \times D_{in}$
2	<i>Conv</i> ($\mathbf{X}_m, D_{in}, D_{out}, \text{stride} = 2$)	$P_m/2 \times D_{out}$
3	<i>BatchNorm</i> (Out(2))	$P_m/2 \times D_{out}$
Upsampling Layer		$\leftarrow \text{Upsampling}(\text{shape repr. } \mathbf{X}_m, \text{in-feat } D_{in}, \text{out-feat } D_{out})$
1	<i>Input: \mathbf{X}_m</i>	$P_m \times D_{in}$
2	<i>TrConv</i> ($\mathbf{X}_m, D_{in}, D_{out}, \text{stride} = 2$)	$2 * P_m \times D_{out}$
3	<i>BatchNorm</i> (Out(2))	$2 * P_m \times D_{out}$
Residual Basic Block		$\leftarrow \text{BasicBlock}(\text{shape repr. } \mathbf{X}_m, \text{\#feats } D)$
1	<i>Input: \mathbf{X}_m</i>	$P_m \times D$
2	<i>Conv</i> (\mathbf{X}_m, D, D)	$P_m \times D$
3	<i>ReLU</i> (<i>BatchNorm</i> (Out(2)))	$P_m \times D$
4	<i>Conv</i> (Out(3), D, D)	$P_m \times D$
5	<i>ReLU</i> ($\mathbf{X}_m + \text{BatchNorm}(\text{Out}(4))$)	$P_m \times D$

Table 4. Cross-Shape Network basic layers. All convolution kernels are of size $3 \times 3 \times 3$.

Category	Bed	Bott	Chai	Cloc	Dish	Disp	Door	Ear	Fauc	Knif	Lamp	Micr	Frid	Stor	Tabl	Tras	Vase	avg.	#cat.
Part IoU																			
MinkHRNetCSN-K1 (Eq. 14)	42.1	54.0	42.5	42.9	58.2	83.2	43.5	51.5	59.4	47.8	27.9	57.4	43.7	46.2	36.8	51.5	60.0	49.9	16
MinkHRNetCSN-K1 (Eq. 10)	38.7	47.0	41.9	40.8	55.7	82.3	41.3	50.5	57.9	37.3	24.7	56.2	44.1	45.9	32.3	51.4	58.8	47.4	1
Shape IoU																			
MinkHRNetCSN-K1 (Eq. 14)	30.5	61.6	50.0	52.1	56.8	83.7	50.8	57.6	66.4	53.4	45.0	60.8	54.4	52.0	47.1	52.5	81.1	56.2	16
MinkHRNetCSN-K1 (Eq. 10)	31.3	57.8	48.2	50.3	55.4	83.0	50.1	56.2	65.0	45.8	43.7	59.8	54.4	51.9	43.5	50.5	76.5	54.3	2

Table 5. Comparison of shape retrieval measures.

Category	Bed	Bott	Chai	Cloc	Dish	Disp	Door	Ear	Fauc	Knif	Lamp	Micr	Frid	Stor	Tabl	Tras	Vase	avg.
DGCNN backbone	33.1	47.5	36.4	22.2	45.7	78.7	23.1	40.6	52.3	28.3	20.0	34.9	28.5	41.2	27.0	43.1	50.7	38.4
DGCNN-CSN-K1	34.7	44.4	34.5	23.2	40.6	78.3	41.8	46.6	51.5	37.8	19.4	41.5	34.1	43.1	29.2	45.8	51.0	41.0
MinkHRNetCSN-K1	42.1	54.0	42.5	42.9	58.2	83.2	43.5	51.5	59.4	47.8	27.9	57.4	43.7	46.2	36.8	51.5	60.0	49.9

Table 6. Comparison between our Cross Shape Network using the DGCNN backbone (“DGCNN-CSN-K1”) versus our Network based on our MinkowskiNet variant (“MinkHRNetCSN-K1”) described in our main text. We also report the performance of the DGCNN backbone (i.e., without cross-shape attention).

a query and a key shape and retrieves key shapes that are on average more similar to their query counterparts (Eq. 14). The second measure, takes into account only the global representations of a query-key pair of shapes

(Eq. 10). In Table 5 we report the performance for both measures, in terms of Part and Shape IoU. Our default variant, “MinkHRNetCSN-K1 (Eq. 14)”, achieves better performance according to both quantitative metrics (+2.5%

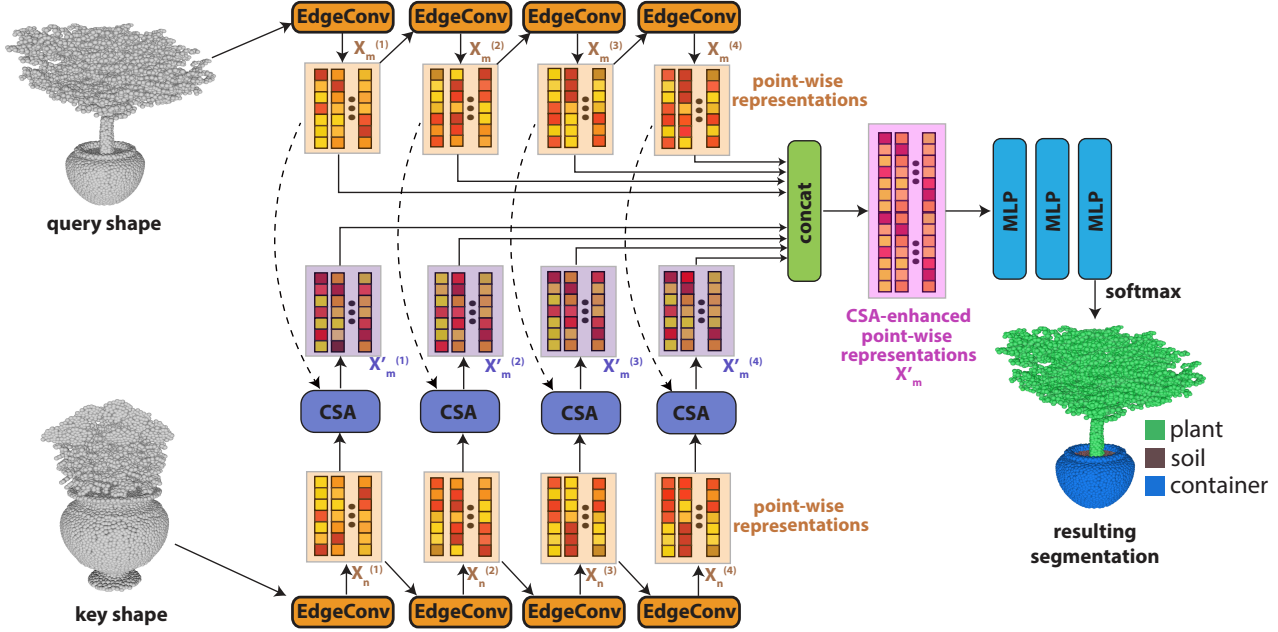


Figure 5. Architecture of our alternative cross-shape attention network using a DGCNN backbone. We demonstrate the cross-attention operations for the case of a query shape shown on the top left and another key shape shown on the bottom left. A sequence of 4 EdgeConv layers [64] paired with our Cross-Shape Attention (CSA) layers process the input points to produce new point representations for the query shape, enhanced by interactions with other points from both shapes.

in Part IoU and +1.9% in Shape IoU), and it outperforms the other variant (“MinkHRNetCSN-K1, Eq. 10”) in 16 out of 17 object categories. This is a strong indication that the key shape retrieval measure based in Eq. 14 is more effective in retrieving key shapes for cross-shape attention.

Appendix C: DGCNN backbone

We now discuss an alternative implementation of our Cross Shape Network using a DGCNN backbone [64]. We visualize our implemented architecture in Figure 5. Given a shape with 3D point positions as input, DGCNN uses a sequence of graph convolution layers, called EdgeConv layers, to output per-point representations $\mathbf{X}_m^{(l)}$ for each EdgeConv layer l . We attach a CSA layer processing the outputs of each corresponding EdgeConv layer. Each CSA layer has its own learned weight matrices specific to each layer. It outputs new point-wise representations stacked in a matrix $\mathbf{X}'_m^{(l)}$ based on Equations 2-6 of the paper. The output representations of the EdgeConv layers along with the ones produced by the CSA layers are concatenated into a single vector \mathbf{X}'_m passed through another 3 MLP layers and a softmax layer for per-point classification.

To train this alternative backbone, we used $2.5K$ points randomly sub-sampled from the original $10K$ points provided for each training shape in PartNet. This resolution is similar to the one used in the original DGCNN for

shape classification and segmentation [64]. We performed this sub-sampling to enable faster training and less GPU memory consumption. Our network and also the original DGCNN network, can handle different number of points as input. Thus, at test time, we process all $10K$ points for test shapes. To perform this direct processing of higher-resolution of point clouds, we needed to perform an adjustment of the receptive field of the DGCNN. During training, our backbone uses $K = 20$ nearest neighbors in its EdgeConv layers. At test time, to achieve a similar receptive field in the higher-resolution point cloud, we increase $K = 20 \rightarrow 80$ at test time (since using the original number of neighbors would result in a smaller receptive field in the higher-resolution point cloud). This adjustment yielded better performance compared to testing on $2.5K$ points then performing upsampling of the per-point classification probabilities to $10K$ points. We note that this adjustment was done only for our architecture based on the DGCNN backbone – our MinkowskiNet variant based on sparse tensors did not need this adjustment to fit in the GPU memory (training and testing were done on the shapes with the original $10K$ points provided in PartNet).

Table 6 reports the Partnet’s Part IoU performance for the DGCNN, our cross-shape network based on the DGCNN backbone (“DGCNN-CSN-K1”) using $K=1$ key shape, and the MinkowskiNet variant (“MinkHRNetCSN-K1”) described in our main text also using $K=1$ key shape.

We note that this comparison is not necessarily fair since our DGCNN backbone was trained on lower resolution (2.5K points) compared to our MinkowskiNet variant. Nevertheless, we observe that our Cross Shape Network based on our MinkowskiNet variant yields significantly better performance compared to using DGCNN as backbone: +8.9% better Part IoU on average, and achieves better results for all 17 tested categories.